ISSN: 2230-9926

Available online at http://www.journalijdr.com

IJDR

International Journal of Development Research
Vol. 10, Issue, 07, pp. 37708-37716, July, 2020
https://doi.org/10.37118/ijdr.19108.07.2020

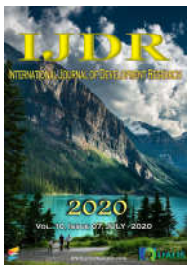

RESEARCH ARTICLE OPEN ACCESS

USE OF INDUSTRIAL AND SOL-GEL CATALYSTS IN THE REMOVAL OF CO FROM AUTONOMOUS FUEL CELLS

Tatiane Caroline Ferrari[1*], João Lourenço Castagnari Willimann Pimenta[2], Mara Heloísa Neves Olsen Scaliante[2], Onélia Aparecida Andreo dos Santos[2] and Luiz Mario de Matos Jorge[2]

[1]Maringá State University, Textile Engineering Department, Brazil; [2]Maringá State University, Chemical Engineering Department, Brazil

ARTICLE INFO

Article History:
Received 10th April, 2020
Received in revised form
17th May, 2020
Accepted 21st June, 2020
Published online 25th July, 2020

Key words:
WGSR, CO, hydrogen, sol-gel.

Corresponding author: Tatiane Caroline Ferrari

ABSTRACT

The low-temperature water-gas shift reaction (WGSR) is already used in several industrial chemical processes. However, interest in this reaction has increased significantly in the last few years because of the advances in fuel cell technology and the need to develop compact reformers for the production of pure hydrogen streams (free from CO). In the present work, the WGSR was carried out on copper-based supported catalysts, one of them already used in the industry and the other one prepared using the sol-gel method with the same composition as the industrial catalyst. The synthesized sol-gel catalyst presented excellent catalytic performance, with a very stable CO conversion of around 60%. The high activity and stability of the sol-gel catalyst were mainly attributed to its large metal surface area and high copper dispersion.

Citation: ***Tatiane Caroline Ferrari, Raphael Menechini Neto, João Lourenço Castagnari Willimann Pimenta et al.*** "Use of industrial and sol-gel catalysts in the removal of co from autonomous fuel cells*", International Journal of Development Research*, 10, 07, 37708-37716.

INTRODUCTION

Fuel cells have been getting more prominent as an interesting option for electricity generation due to their high efficiency when converting chemical energy from the fuel (hydrogen) directly into electrical energy (Nepel, 2013). Hydrogen is the simplest and most abundant element in the universe, being found in our planet mainly in hydrocarbons and in water. Its energy-per-mass ratio of 120.7 kJ g^{-1} surpasses that of any other fuel (Sanches, 2009). According to Sanches (Sanches, 2009), hydrogen can be produced through different processes from natural gas, petroleum, hydrocarbons, coal, biomass, and municipal solid waste. An interesting means of production uses the methanol steam reforming. In this process, however, a significant amount of carbon monoxide is present in the hydrogen stream, causing electrode poisoning in the PEM (Proton Exchange Membrane) fuel cell, thus reducing its efficiency. In the last few years, a lot of attention has been given to the water-gas shift reaction (WGSR), which is shown in Eq. (01), for the removal of CO from the hydrogen-rich stream generated through reforming. This stream is then used in autonomous fuel cells (3-5). The challenges in the production and use of hydrogen as fuel, however, are still great, resulting from the need to obtain pure hydrogen streams. Therefore, autonomous fuel cells are usually designed by associating a reforming reactor with a fuel cell and interposing a CO removal system. The catalyst $Cu/ZnO/Al_2O_3$ is industrially used in the WGSR and, therefore, is already produced by several industries, such as Alfa Aesar, which produces HiFUEL W220.

$$CO + H_2O \rightleftharpoons CO_2 + H_2\ ,\ \Delta^{\circ}_{298}H = -41{,}1\ kJ\ mol^{-1} \qquad (1)$$

However, little is known about the use of such catalysts to reduce CO content in fuel cells. This is because, even though this reaction is widely studied, few citations of its use exist in the literature (Wijayapala, 2014; Liang, 2012) and even less citations exist for the sol-gel catalyst used in that system. Many catalysts have been recently explored for the low-temperature WGSR by varying the copper composition and the support materials (Jeong, 2014; Nishida, 2008; Fu, 2011). The catalytic activity in this reaction depends on countless factors including preparation method, nature of the support material, test conditions, and reactor configuration (Hakeem, 2015; Colussi, 2014). However, since the performance of Cu-based catalysts relies heavily on the preparation method (Jeong, 2014; Colussi, 2014), less common preparation methods for catalysts have been found interesting by several research

groups. Catalysts obtained through the sol-gel method, also known as chemical solution deposition, are more active and more selective, besides forming a lower amount of coke and showing greater thermal stability when used in many heterogeneous catalytic reactions (Gonçalves, 2013; Colpini, 2013). This high performance is due to a collection of important characteristics presented by said catalysts, such as high porosity, homogeneity, and specific surface area. However, the literature does not present any references to the use of this method in the synthesis of $Cu/ZnO/Al_2O_3$-based catalysts for use in the WGSR. Therefore, a decision was made to compare a catalyst already used in the industry (HiFUEL W220) with a catalyst with the same composition synthesized through the sol-gel method and to verify the conversion of CO for each one of them using tests of long and short duration. Both catalysts were characterized by TGA-DSC, BET, XRD, s-TPR, TPR, FTIR, SEM, and TEM. The results were related to the activity results for the WGSR. The formation of coke was also identified by SEM and quantified through a carbon balance.

Experimental

Properties of the commercial catalyst: The industrial catalyst used in the experiments was HiFUEL W220 produced by Alfa Aesar®, Johnson Matthey. The physicochemical properties, which were provided by Alfa Aesar's Certificate of Analysis (Production Lot B11T010), are found in Table 1.

Table 1. Physicochemical properties of the catalyst HiFUEL W220

Property	Value
Average length	3.4 mm
Average vertical crushing resistance	66 kgf
% that breaks under 20 kgf	< 1%
Loss on ignition	6.0%
Density	1.40 kg L^{-1}
Composition	

Synthesis of the sol-gel catalyst: The sol-gel catalyst was synthesized following the methodology proposed by Pearson et al. (14) and modified by Santos (15) and Lenzi et al. (16), keeping the copper/zinc mass ratio constant at 1.66 (Cu/Zn mass ratio of the catalyst HiFUEL W220). 10 mL of ethanol (Nuclear, purity > 99.5%) were added to a magnetically stirred beaker, followed by the addition of copper nitrate trihydrate ($Cu(NO_3)_2.3H_2O$, Sigma-Aldrich, > 99%) and zinc nitrate hexahydrate ($Zn(NO_3)_2.6H_2O$, Sigma-Aldrich, > 99%). Enough ethanol was then added to dissolve both salts completely. This solution was then transferred to a three-necked flask immersed in a glycerin bath. The flask was connected to a mechanical stirrer, a condenser (traversed by running water at room temperature), and a dropping funnel. The glycerin bath stood over a heating plate and its temperature was controlled using a digital thermometer. The transferred solution was stirred for 15 min at room temperature. After the heating was turned on, hexylene glycol (Sigma-Aldrich, 99%) was slowly added using the dropping funnel. The hexylene glycol acted as a solvent for the precursor of alumina, being added at a hexylene glycol/aluminum isopropoxide mass ratio of 1.16. When the glycerin bath reached a temperature of 95 °C, the mixture was left under stirring for 30 min. Aluminum isopropoxide (Sigma-Aldrich, 98%) was then added using a funnel. The mixture was left under stirring at 95 °C for 4 h. The hydrolysis step was next, where a 1:1 (v/v) solution of ethanol and water was slowly added using the dropping funnel until a water/aluminum isopropoxide molar ratio of 4.5 was achieved. The mixture was stirred for a further 3 h. After being cooled, the flask was left to age, closed and at room temperature, for 85 h. In this step, the particles and crystallites of the active phase are organized and ordered due to the contact with the mother liquor. After the aging period, the obtained gel was submitted to a pre-drying process in a rotary evaporator. This process of evaporation under reduced pressure was carried out for 90 min at 70 °C to remove excess solvents (water and ethanol). By the end of this process, the catalyst (gel) was placed in an air circulation oven at 70 °C for 48 h, being then left in the desiccator for a further 48 h. The gel was submitted to high-vacuum drying for 16 h to remove nitrates, hexylene glycol, and possible solvent residues. The temperature was gradually raised (6 h at 70 °C, 6 h at 100 °C, and 4 h at 150 °C) in order to remove first the solvents with low boiling points and, with the subsequent rise in temperature, the hexylene glycol, which has a higher boiling point (197 °C). This prevents excessive formation of liquid on the surface of the solid inside the flask, which is important to prevent a possible drag of said formed liquid into the high-vacuum line. The catalyst was then removed from the high-vacuum drying system and stored in a covered glass container.

Catalyst characterization

The characterization of the catalysts was carried out using crushed and sifted particles of diameters 0.6 mm < d < 0.85 mm, except in X-ray diffraction (d < 0.6 mm).

- Obtaining the metal compositions
- The metal compositions were obtained through atomic absorption spectrometry (Varian, Atomic Absorption Spectrometer SpectrAA 50B) after the dissolution of the sample through acid digestion on a hot plate.
- Thermogravimetric Analysis (TGA) and Differential Scanning Calorimetry (DSC)
- The TGA and the DSC were carried out in a NETZSCH STA 449 F3 Jupiter® simultaneous thermal analyzer. In this analysis, approximately 29 mg of the catalyst sample were submitted to heating from room temperature to 920 °C at a rate of 10 °C min^{-1}. Nitrogen was the carrier gas of choice, passing through the chamber at a flow rate of 20 mL min^{-1}.
- BET area, pore volume, and mean pore diameter
- These variables were determined using the software NovaWin version 10.01, after nitrogen adsorption measurements in the equipment QUANTACHROME NOVA 1200.
- Temperature-programmed reduction (TPR)

The TPRs were carried out in a home-made equipment at the Department of Chemical Engineering – UEM. A sample from the catalyst with a known mass was placed in a U-shaped quartz reactor on a porous plate and heated from room temperature to 1000 °C at a rate of 10 °C min^{-1} and a gas flow rate of 20 mL min^{-1} (1.75% H_2 and 98.25% Ar).

X-ray diffraction (XRD): X-ray diffractograms of the calcined samples were obtained in a BRUKER D8 Advance Diffractometer using a copper anode and Kα radiation (V = 40 kV, I = 35 mA).

TPR of oxidized surfaces (s-TPR): The s-TPR measurements allow the calculation of the metal surface area (MSA), the dispersion (D_{Cu}), and the average particle size (ϕ) of copper (17). The s-TPR was carried out in the Quantachrome ChemBET™ TPR/TPD connected to a Pfeiffer vacuum Thermostar™ mass spectrometer. The reduction of the catalyst was carried out in a flow of 1% H_2/He with a rate of 30 cm³ min^{-1} using a heating rate of 10 °C min^{-1} from room temperature to 350 °C. To reoxidize the surface under mild conditions, a mixture of 30% N_2O/He was used at 60 °C. Finally, the reduction was made using a mixture of 1% H_2/He with a flow rate of 30 cm³ min^{-1}. Scanning electron microscopy: Surface micrographs of the sol-gel catalyst sample prior to calcination were obtained in a TESCAN VEGA3 LMU microscope located in the electron microscopy center of the Federal University of Paraná (UFPR) using an EDS chemical analysis system (Oxford) with AZ Tech software (Advanced) and an 80mm² SDD detector. Surface micrographs of the sample after calcination and after the reaction were obtained using scanning electron microscopy (SEM) in a Shimadzu SuperScan SS-550 microscope located in the complex of research support centers (COMCAP/UEM).

Transmission electron microscopy: Surface micrographs of the catalyst sample after calcination were obtained using transmission electron microscopy (TEM) in a JEOL JEM-1400 microscope with tungsten filament and using the phase contrast from the complex of research support centers (COMCAP/UEM).

Infrared spectroscopy: Fourier transform infrared spectroscopy (FTIR) analyses were carried out in a Bruker Vertex 70V spectrometer. Catalytic tests: After the synthesis of the sol-gel catalyst and the characterization of both catalysts, the catalytic tests would determine whether they were viable for a given reaction of interest. Therefore, long-duration (12 h) and short-duration tests were carried out in order to investigate the influence of the temperature and of the CO/steam molar ratio on the conversion. Experimental data was obtained in the reaction unit presented in Figure 1, which is made up of five basic parts. Gas feeding (storage cylinders); liquid feeding (water), carried out using a pump; reaction unit, consisting of a microreactor housed inside an electrically-heated oven and a thermocouple to control the temperature; separation of condensable substances (condenser and phase separator); and chromatographic analysis, responsible for the identification and quantification of both the liquid and the gaseous products. The microreactor consists of a tube containing a very small amount of catalyst (500 mg). This catalyst was placed over a stainless steel screen with openings smaller than the particle size (0.65 – 0.80 mm).

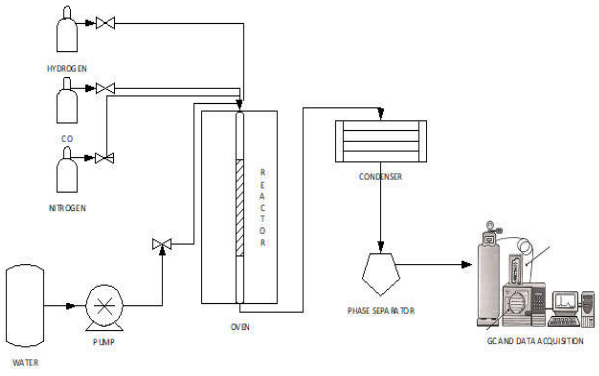

Figure 1. Schematic diagram of the reaction unit

Prior to the reaction, the catalyst was dried with nitrogen under constant heating to remove possible contaminants. The step that follows the drying process, catalyst activation, was then started. In this step, the N_2 was substituted by a 5% H_2, 95% N_2 flow together with gradual heating from room temperature to 400 °C, staying at that temperature until complete reduction of the metal oxides that make up the catalyst. After the activation step has been carried out, simultaneous injection of water and CO has to be avoided, as it could lead to oxidation of the catalyst. To bypass this problem, the water intake must be kept at a certain ratio relative to hydrogen such that a reductive atmosphere is secured for the catalytic material (18). Therefore, instants after the water arrived in the phase separator the flow of the mixture (H_2 + N_2) was replaced by the CO flow at a pre-determined rate. The reaction was conducted at 200 °C with a water flow rate set at 243 mL min^{-1} (keeping the CO/steam ratio at 1/2) (3). N_2 was also added as a diluent (fixed flow rate of 100 mL min^{-1}) due to the high toxicity of CO, making working with high flow rates of said gas dangerous. The resulting WGSR products were analyzed by gas chromatography (GC). The gaseous products that could be found were CO, CO_2, H_2, and CH_4 (19). The liquid products were collected in the phase separator and analyzed, showing the presence of methanol and formaldehyde (19, 20).

RESULTS AND DISCUSSION

Synthesis of the sol-gel catalyst: During the high-vacuum drying of the sol-gel catalyst, two relevant events were observed:

- The formation of dinitrogen trioxide (N_2O_3), a blue solid residue at low temperatures, observed inside the trap system for solvents and other residues (Figure 2a).
- After the trap reached room temperature, the N_2O_3 turned into a light-brown gas, which was identified to be nitrogen dioxide, NO_2, an acrid, highly toxic yellow-brown gas (Figure 2b).

The formation of such compounds demonstrates sublimation and decomposition of the nitrate, which originates from the precursor salts, present in the catalyst.

Composition of the sol-gel catalyst: The percentages and ratios of the components present in the catalysts are presented on mass basis in Table 2. It is evident that, generally speaking, the catalysts had very similar compositions. HiFUEL W220, however, presented a slightly higher metal content.

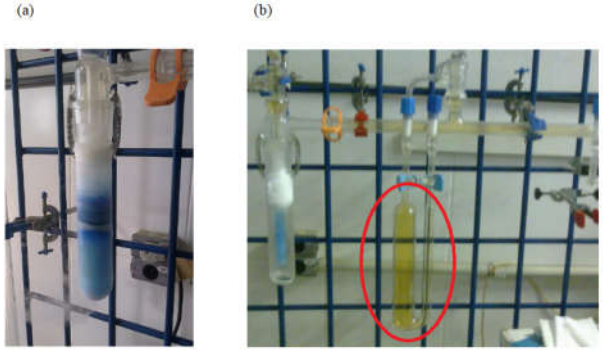

Figure 2. (a) Trap system for solvents and other residues and (b) Dinitrogen trioxide, N2O3, blue in the left trap, turning into nitrogen dioxide, NO2, maroon in the center trap (circled).

Table 2. Composition of the catalysts.

Catalyst	%Cu	%Zn	%Al	Cu/Zn Ratio	Cu/Al Ratio	Zn/Al Ratio
Sol-gel	40.6	23.1	9.0	1.76	4.52	2.57
W220	41.9	24.9	9.0	1.68	4.66	2.77

TGA-DSC: The catalyst HiFUEL W220 (Figure 3) presented a loss of mass of approximately 12 % in the analysis carried out from room temperature to 950 °C, which is a very small amount. This loss of mass is due to different factors. Around 4% of the mass is lost in the transition from room temperature to 400 °C, possibly due to the presence of physisorbed water in the catalyst or in its structure. Another possibility is decomposition, since it happens for copper nitrate and copper hydroxide at 160-230 °C, according to the literature (Fu, 2011; He, 2013). Another notable loss of mass of approximately 4% happens around 720 °C, which can be attributed to the release of trace residues of materials used during the preparation of the catalyst pellet, such as binders and organic lubricants. The rest of the mass was lost gradually throughout the process. A small increase in mass is also noticeable in Figure 3 right at the beginning of the reaction, at temperatures between 40 and 70 °C. This increase can be related to the oxidation of the metal phases into their corresponding oxides (Chu, 2013). According to Figure 3, a phase transition happens at approximately 717 °C for HiFUEL W220. However, since the reaction temperature would be 200 °C (low-temperature WGSR), the calcination could be carried out at 400 °C.

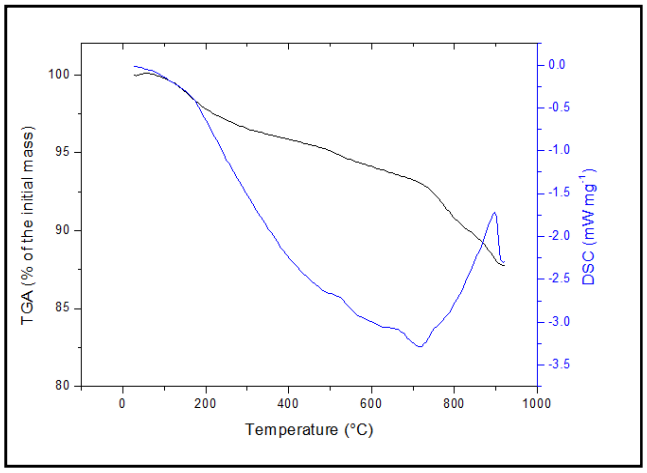

Figure 3. TGA and DSC of the catalyst HiFUEL W220 (—TGA and — DSC)

It is clear from the TGA curve shown in Figure 4 that the decomposition of the sol-gel catalyst happens at three separate temperature regions. The first loss of mass (11%) happens from 50 °C to 250 °C and corresponds to physisorbed water in the catalyst. The second loss of mass (30%) happens from 250 °C to 350 °C and it can be attributed to decomposition of the nitrates and carbonization of residual solvents. The third loss of mass (approx. 4%) happens from 350 °C to 900 °C and originates from the evaporation of residual solvents (hexylene glycol) and from the continuous pyrolysis of organic residues (Shi, 2011; Lei, 2012). The sol-gel catalyst presented a loss of mass of approximately 45% in the analysis carried out from room temperature to 950 °C, which is a much higher figure than the 12% lost by the industrial catalyst. According to Figure 4, a phase transition happens in the sol-gel catalyst at approximately 250 °C and another at approximately 350 °C. The DSC presented in Figure 4 corroborates that the decompositions undergone by the catalysts are endothermic, as reported in the literature (Shen, 1997; Porta, 1998; Kanari, 2004). The exothermic peak, on the other hand, may be related to a martensitic transformation (crystal deformation) after the aging process (Nakata, 1993). The calcination of this catalyst was carried out at 400 °C, a temperature that was chosen because at this point the necessary transitions have already occurred and most precursors have already been decomposed.

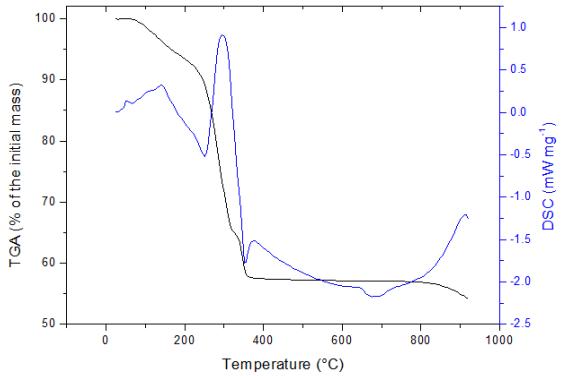

Figure 4. TGA and DSC of the sol-gel catalyst (—TGA and — DSC)

BET Area, Total Pore Volume, and Mean Pore Diameter: The results of the textural characterization are shown in Tab. 3 for both analyzed catalysts, with the one synthetized through the sol-gel method being analyzed in two forms: pelleted (P) and non-pelleted (NP). The pelleting of the catalyst was carried out by applying a pressure of 3 ton (LEMAQ Monopress LM-1 compressing machine).

Table 3. Textural analysis of the catalysts

Catalyst		BET Area ($m^2\ g^{-1}$)	Total pore volume ($cm^3\ g^{-1}$)	Mean pore diameter (Å)
Sol-gel	P	65.8	0.070	42
	NP	94.0	0.403	171
W220		96.57	0.106	43.98

The micropores present diameters that range from 0.3 to 2 nm, while the mesopores range from 2 nm to 50 nm (Schmal, 2011). Therefore, it can be concluded that both analyzed catalysts are mesoporous. Relative to Table 3, it can be observed that the pelleting reduced the surface area, the volume, and the diameter of the pores of the sol-gel catalyst. This happens due to the compression of the particles that constitute the catalyst. Tanaka et al. (2003) prepared a catalyst through the co-precipitation method with 30 wt.% Cu/ 30 wt.% ZnO/40 wt.% Al_2O_3 and obtained a BET surface area of 118 $m^2\ g^{-1}$. According to the authors, the BET surface area simply lowered with an increase in the copper and the zinc oxide contents, which might explain the area presented by the catalyst HiFUEL W220, since said contents are higher in this catalyst.

A $Cu/ZnO/Al_2O_3$-based catalyst was synthesized through the sol-gel method by Panyad et al. (2011) and presented a BET area of 175 $m^2\ g^{-1}$, a pore volume of 0.395 $cm^3\ g^{-1}$, and a pore diameter of 6.18 nm after pelleting. These values are very different from those presented in Table 3, which can be justified if the copper percentage used by the authors, which was much lower than that used in the present study, is taken into account. It is important to consider that HiFUEL W220 is a catalyst already used by the industry. According to the

manufacturer, catalysts from the HiFUEL line present a characteristic high geometric surface area, which allows the reactants to have an excellent access to active sites on the surface of the catalyst.

XRD: The diffractograms for both catalysts used are presented in Figure 5, confirming that the Cu-Zn-Al_2O_3 phases of the synthesized sol-gel catalyst in the present work are virtually the same found in the commercial one. However, it is evident that the catalyst prepared through the sol-gel method presents more ample and more well-defined CuO, ZnO, and Al_2O_3 peaks, indicating superior cristallinity of the sol-gel catalyst relative to the commercial one.

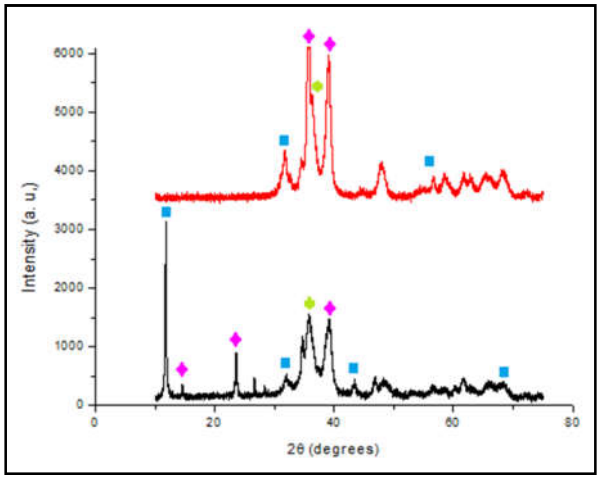

Figure 5. X-ray diffractograms of the catalysts: (—) HiFUEL W220 and (—) sol-gel, where (■) Al_2O_3, (♦) CuO, and (●) ZnO.

Both the industrial HiFUEL W220 and the sol-gel catalysts presented well-defined characteristic Al_2O_3 peaks, showing that it is found in crystalline form. This same result was described for a commercial Cu/Zn/Al_2O_3 catalyst (Süd-Chemie AG, Munich, Germany) (Henpraserttae, 2010).

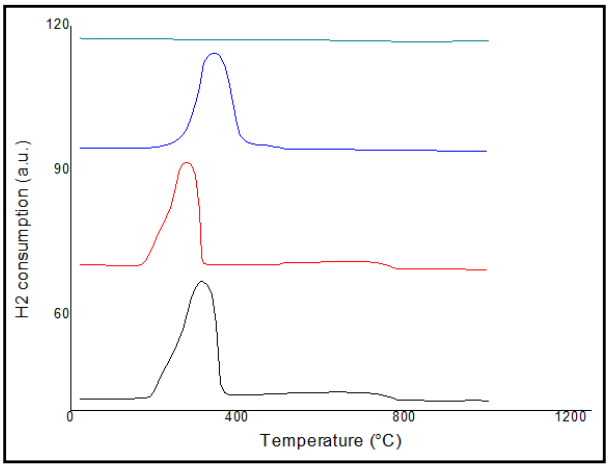

Figure 6. TPR profiles of the catalysts and oxides (— ZnO, — CuO, — HiFUEL W220, and — sol-gel).

TPR: According to Figure 6, the copper oxide undergoes reduction tenfold relative to the zinc oxide. Both analyzed catalysts (HiFUEL W220 and sol-gel) presented TPR profiles with a well-defined reduction peak, with maximum reduction around 190-320 °C. This behavior was also reported by several authors (Fierro, 1996; Agrell, 2002). Catalysts with high Cu/Zn ratios present, in the TPR, individual and narrow reduction peaks, though these peaks are centered on lower temperatures than those for pure CuO (35), as can be observed in Figure 6. The reduction of the HiFUEL W220 catalyst is completed at a lower temperature than that of the sol-gel catalyst. However, the peak of the sol-gel is broader than that of the industrial catalyst. This shows that the sol-gel catalyst has a higher amount of reducible species relative to both CuO and ZnO.

Table 4. Amount of reducible species, in mol g^{-1} of catalyst

Catalyst	HiFUEL W220	Sol-gel
CuO	$5.26.10^{-3}$	$5.46.10^{-3}$
ZnO	$5.84.10^{-4}$	$6.71\text{-}10^{-4}$

Table 4 shows that the amount of reducible species relative to CuO is very similar for both catalysts, while the amount relative to ZnO is higher for the sol-gel catalyst. According to Jeong et al. (2014), the performance of the supported Cu catalysts strongly depends on the reducibility of the catalyst. Thus, the sol-gel catalyst is expected to present a better performance in CO conversion, since it favored the formation of species that are more reducible on the surface of the catalyst.

s-TPR: Some important characteristics of the sample, such as the copper metal surface area (MSA), the mean copper particle size (5), and the copper metallic dispersion (D_{Cu}), are presented in Table 5.

Table 5. Some textural and structural properties of the studied catalysts

Catalyst	MSA ($m^2\ g^{-1}$)	ϕ (nm)	D_{Cu}
HiFUEL W220	70.05	9.60	0.08
Sol-gel	272.22	2.47	0.35

It is evident, from Table 5, that the sol-gel catalyst presents a much larger copper metal surface area when compared with HiFUEL W220. Furthermore, the copper particle diameter was much smaller for the sol-gel catalyst, which may suggest that the copper particles are much more scattered in the sol-gel catalyst than in the commercial one. This is noticeable from the metallic dispersion analysis (D_{Cu}). Results similar to those in Table 5 were presented by Pernicone et al. (36) for four commercial catalysts used in the low-temperature WGSR. These catalysts had a mean copper particle diameter of 7.33 nm (from 3.8 to 13.8 nm), a mean copper surface area of 127 $m^2\ g^{-1}$ (from 41 to 149 $m^2\ g^{-1}$), and a mean copper dispersion of 0.1475 (from 0.06 to 0.23). However, the methodology used in the analysis was different from that used in the present work (section 2.3). MSA values between 278 and 481 $m^2\ g^{-1}$ are found in the literature (Gervasini, 2005) for copper particles in the order of 20 nm in Cu/Zn/Al_2O_3 catalysts produced through impregnation. These values are notably similar to that obtained for the sol-gel catalyst. Results for the size of the copper particle match those presented for the XRD, since the higher presence of peaks referent to CuO for the sol-gel catalyst can be attributed to the bigger size of the copper particle in this catalyst.

Fourier Transform Infrared spectroscopy: The FTIR profile was similar for both catalysts. The presence of several complex organic compounds, rich in carbon, hydrogen, and oxygen, can be identified. Such compounds might come from other materials used in the synthesis, as is the case for the

industrial catalyst, or from any residues or modifications from the precursors. Some authors, however, note that, in the spectrum corresponding to the CuO-ZnO-Al_2O_3 metallic function, the bands corresponding to CuO and to ZnO appear in the 1000-4000 cm^{-1} range, though they overlap the bands corresponding to Al_2O_3 (Ereña, 2008).

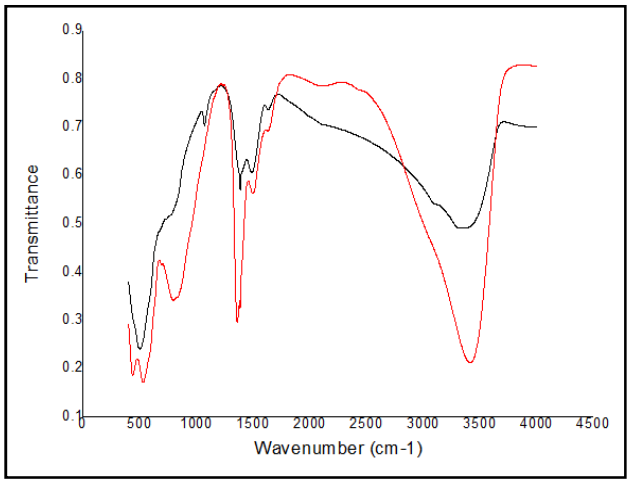

Figure 7. Infrared spectroscopy of the catalysts: (—) HiFUEL W220 and (—) sol-gel

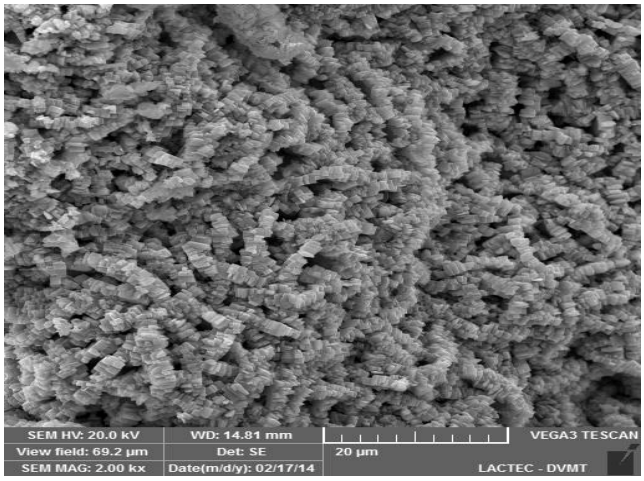

Figure 8. SEM micrograph of the sol-gel catalyst before calcination, 2000x magnification

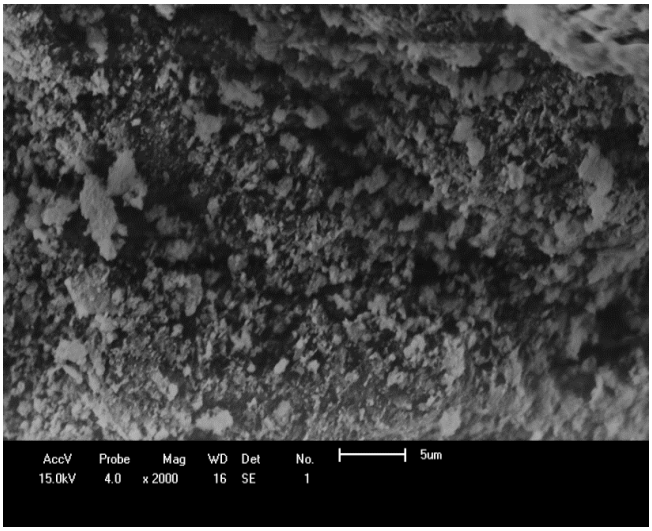

Figure 9. SEM micrograph of the sol-gel catalyst after calcination, 2000x magnification

Scanning Electron Microscopy (SEM): The SEM analysis was carried out for the sol-gel catalyst before and after calcination (pelleted and calcined), as well as for the HiFUEL W220 commercial catalyst. The results are shown in Figures 8 to 10. Results obtained through SEM analysis of the non-calcined sol-gel catalyst show a stacked lamellar structure where the particles are orderly, uniform, and grouped in filaments.

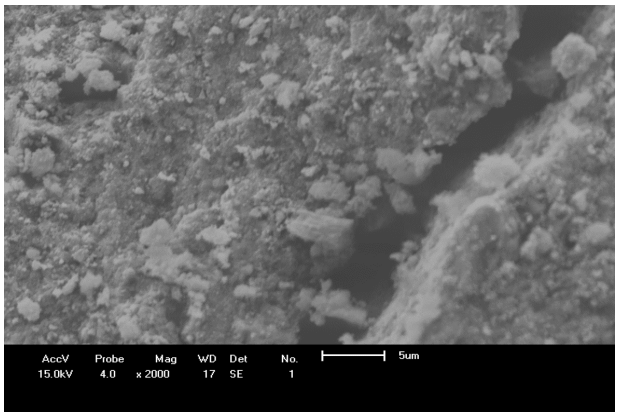

Figure 10. SEM micrograph of the HiFUEL W220 catalyst, 2000x magnification

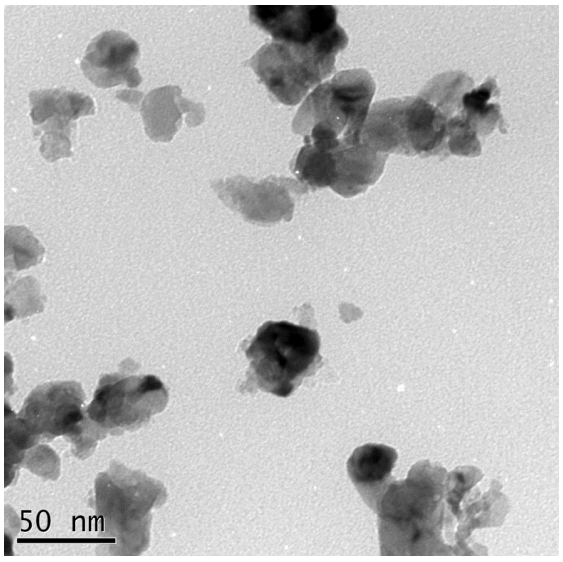

Figure 11. TEM micrograph of the Cu/ZnO/Al_2O_3 sol-gel catalyst, 300k magnification

On the other hand, results for the calcined catalyst (Figure 9) show a clear change in the morphology of the analyzed material, whose orderly structure is undone. Furthermore, there is a notable clustering of the structures on the surface of the catalyst. Therefore, it can be concluded that the calcination process significantly changed the morphology of the catalyst, turning an orderly, lamellar, filamentous structure into a clustered one. The formation of these clusters is probably due to the sintering process of smaller crystals into larger ones (partial fusion, recrystallization, and crystal growth) caused by the high temperature used in the calcination (400 °C). Figure 10 shows that the HiFUEL W220 catalyst presents a structure that is more massive, with less formation of said agglomerations. This may suggest a lower catalytic activity in this material. Henpraserttae et al. (2010) analyzed the surface of a commercial Cu/Zn/Al_2O_3 catalyst (Süd-Chemie AG, Munich, Germany), prepared using the precipitation method at a respective ratio of 40/30/30, using scanning electron

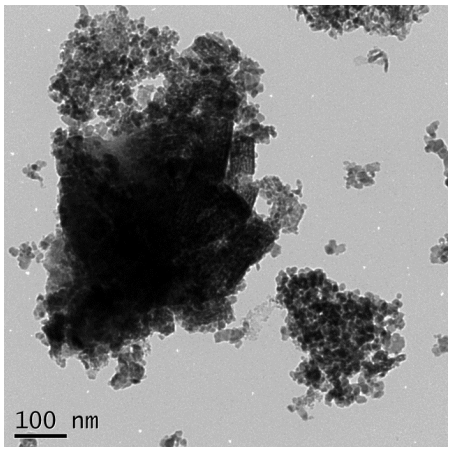

Figure 12. TEM micrograph of the HiFUEL W220 catalyst, 120k magnification

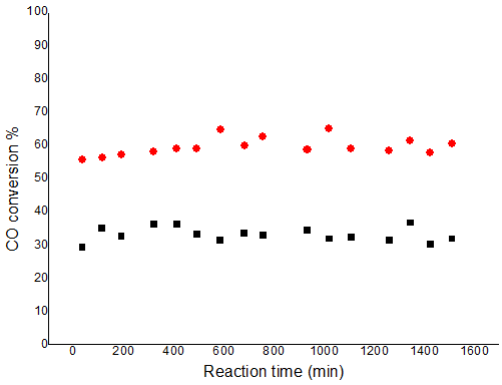

Figure 13. CO conversion profiles of the catalysts HiFUEL W220 (■) and sol-gel (●) as functions of time

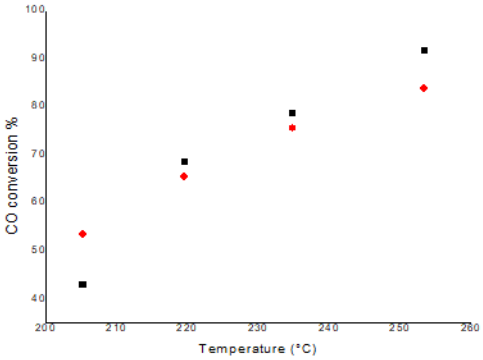

Figure 14. Profile of the CO conversion for the short-duration test (CO/steam molar ratio = 1/2) (■ HiFUEL W220 and ♦ sol-gel)

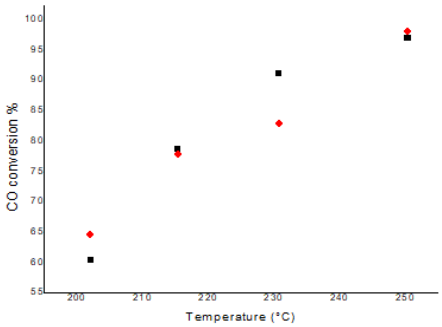

Figure 15. Profile of the CO conversion for the short-duration test (CO/steam molar ratio = 1/3) (■ HiFUEL W220 and ♦ sol-gel)

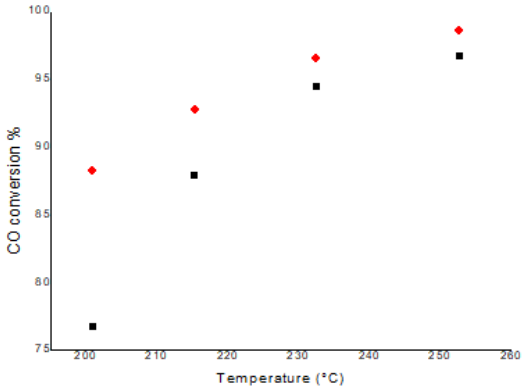

Figura 16. Profile of the CO conversion for the short-duration test (CO/steam molar ratio = 1/4) (■ HiFUEL W220 and ♦ sol-gel).

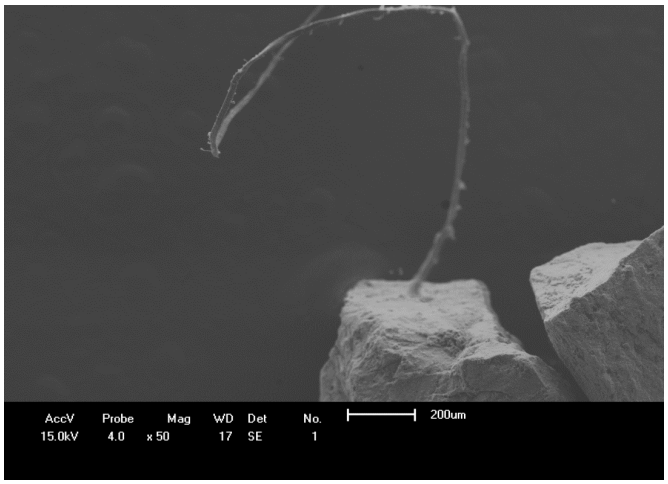

Figure 17. SEM micrograph of the HiFUEL W220 catalyst after its use in the reaction, 50x magnification.

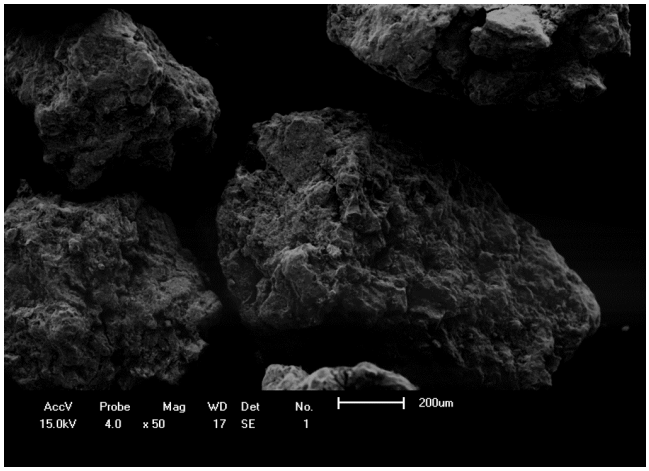

Figure 18. SEM micrograph of the sol-gel catalyst after its use in the reaction, 50x magnification

Table 6. Errors obtained in the carbon balance from the reaction data (long-duration tests)

Catalyst	E (%)
HiFUEL W220	50.75
Sol-gel	14.19

microscopy. The images showed that Cu, Zn, and Al were well mixed along the whole catalyst, without the formation of any separate metallic clusters. The result obtained by these authors

is very similar to that presented in Figure 10, which leads to the conclusion that the Cu, Zn, and Al species are present contiguously on the surface of the catalyst.

Transmission Electron Microscopy (TEM): The image obtained for the sol-gel catalyst using TEM shown in Figure 11 illustrates the typical microstructure of this catalyst: several similar clusters with sizes ranging from 10 to 100 nm. The ZnO particles (lighter color) serve as separators for the Cu particles (darker color), preventing them from sintering. The Cu particles are frequently in contact with several ZnO particles, which can also be observed in Figure 11. It is also visible that most Cu particles show a round shape, similar to an ellipsoid or a sphere. These shapes are usually related to the atomic position coordinates of a copper unit cell (Wang, 2016). The mean Cu particle size was determined measuring the projected individual particle areas in the TEM images. In Figure 11, near the center, a copper particle of approximately 25 nm (half the scale used) is evident. This value is, according to the measurements taken, an average of the diameters of the copper particles in the sample. According to ASTM (39), nanoparticles, either manmade or natural, are materials with at least two dimensions between 1 and 100 nm. Therefore, the synthesized sol-gel catalyst can be labeled as a material that contains copper nanoparticles in its surface. It is evident, in the image obtained for the industrial catalyst using TEM, shown in Figure 12, that the microstructure of this material is formed by several clusters with sizes ranging from 10 to 300 nm.

The ZnO particles in the industrial catalyst (lighter color) also serve as separators for the Cu particles (darker color). However, they end up being engulfed by the wide clusters of Cu. Furthermore, the Cu particles have a noticeably round shape, except for the larger particles. The average particle size of Cu was also determined by measuring the projections of the areas of individual particles on the TEM images, resulting in a size of 325 nm. Thus, the industrial catalyst cannot be considered to be a nanomaterial.

Long-duration tests: Figure 13 shows the behavior of carbon monoxide conversion as a function of time for both catalysts, totaling 12 hours of reaction time. The temperature was kept at 200 °C and the CO/steam molar ratio was 1/2. It is evident that both catalysts presented very stable activity, showing virtually linear behavior during the whole reaction process. Another $Cu/Zn/Al_2O_3$-based catalyst presented in the literature, prepared through coprecipitation with Cu : Zn : Al = 1 : 0.8 : 0.2, has shown very stable activity in 4 h operation at steady state at 250 °C (3), which corroborates the results in the present work. However, the sol-gel catalyst presented a much higher conversion (around 60%) than that of the HiFUEL W220 catalyst (around 35%). In the GC analysis, which was carried out for both the HiFUEL W220 and the sol-gel catalysts, the compounds that were identified by the chromatograms were H_2, N_2, CO, and CO_2. No methane (CH_4) was formed. In the GC analysis carried out for the liquid product only water, which is the excess reactant, was detected.

Short-duration tests: The temperatures used for testing with both catalysts were 200, 215, 230, and 250 °C. The CO/steam molar ratios were 1/2, 1/3, and 1/4. Figures 14, 15, and 16 present the behavior of the carbon monoxide conversion as a function of time for both the HiFUEL W220 and the sol-gel catalysts. It is notable, from the analysis of the figures above, that lowering the CO/steam ratio increases the conversion of carbon monoxide. This behavior is easy to explain, since a lower amount of CO entering the system makes its conversion easier, given that excess water favors the formation of H_2. This behavior is visible for both the HiFUEL W220 and the sol-gel catalysts. The obtained results were similar to those from Figueiredo et al. (2005), whose work show similar CO conversion profiles for the WGSR when using an industrial catalyst (called IND) and one prepared using coprecipitation. The conversion of CO increased continuously with an increase in the steam/carbon molar proportion until a virtually constant value was achieved. Similar results were also presented by Guo et al. (2009). It is also worth of note, from the analysis of the figures, that the sol-gel catalyst presents, at low temperatures (200 °C), better results than HiFUEL W220. However, with increasing temperatures, the presented CO conversions are virtually the same for both catalysts. It is important to highlight that, although the BET area of the sol-gel catalyst was lower than that of the industrial one, the response to the CO conversion was still better for the sol-gel catalyst. This may be due to the considerably higher copper surface area (MSA) of the sol-gel catalyst relative to the industrial one.

Analysis of coke formation: Figure 17 shows the result of the SEM for the HiFUEL W220 catalyst after its use in the long-duration test reaction. Figure 18 shows the result for the sol-gel catalyst. While filamentous structures, which seem to be "leaving" the catalyst, clearly appear in HiFUEL W220, the same does not happen in the sol-gel catalyst. Such structures were not detected in the analysis carried out prior to the reaction, leading to the conclusion that they are a consequence of the reaction process to which HiFUEL W220 was submitted, being identified as filamentous coke. This type of coke usually does not lead to quick deactivation of the bed (40), which may justify the virtually stable activity of the sol-gel catalyst throughout the process (Figure 13). According to Oliveira (19), the formation of coke (C) in the WGSR can be explained by the occurrence of reactions parallel to the CO reduction. Such reactions are represented by Equations 02 and 03.

$$CO + CO \rightarrow CO_2 + C \quad (2)$$

$$CO + H_2 \rightarrow C + H_2O \quad (3)$$

Due to an unavailability of equipment to carry out the SEM for the sol-gel catalyst after the reaction, a carbon balance was carried out in the data collected from the long-duration tests. The error of the molar carbon balance was calculated using Equation 04.

$$E(\%) = \left(1 - \frac{F_{CO}+F_{CO_2}}{F_{CO}^0}\right).100 \quad (4)$$

Values were obtained for F_{CO} and F_{CO_2}, which are the concentrations of CO and CO_2, respectively, in the gas produced in the reaction. F_{CO}^0 is the inlet concentration of CO. The difference obtained in the carbon balance was assumed to be due to the formation of coke, that is, the error shows the quantity of carbon that did not remain as CO, nor was transformed in CO_2. Table 6 presents and compares the mean values obtained for the formation of coke for the HiFUEL W220 and the sol-gel catalysts. From the molar balance of the compounds present in the reaction system, the formation of

coke was assumed to have happened for both catalysts. It was, however, much more significant in the HiFUEL W220. The lower formation of coke also helps to explain the higher conversion obtained in the long-duration test with the sol-gel catalyst. Since conversion was constant for both catalysts during the long-duration tests, it may be presumed that the formation of filamentous coke happened for both the HiFUEL W220 (which was proven by SEM) and the sol-gel catalysts. Gonçalves et al. (2013) had already obtained similar results for a Ni/Al_2O_3 catalyst used in dry methane reforming. In this case, the formation of coke was equivalent for both synthesized catalysts (one using the impregnation method and the other the sol-gel method). However, conversion was constant for the catalyst prepared using the sol-gel method for the totality of the long-duration test.

Conclusion

During characterization, it became clear that the catalyst synthesized using the sol-gel method presents some advantages, such as higher cristallinity, greater metal surface area, lower copper dispersion, smaller copper particle size, and lower formation of coke. However, when the results presented by the BET analysis are evaluated, it becomes clear that the greatest characteristic of the sol-gel catalyst, which is to yield materials with a large area, was lost due to the high percentage of copper in the composition of the catalyst. Nevertheless, this characteristic did not reflect on the results of the catalytic test. Between the analyzed catalysts, the one that presented the best results for CO conversion was the sol-gel. It can be stated that the significantly greater copper area when compared with that of the industrial catalyst may have compensated for the smaller BET area. The results of the catalytic tests confirm that the sol-gel catalyst is very promising for the development of reactors for CO removal using the WGSR, aiming at the use in PEM fuel cells.

Acknowledgements

The authors would like to thank the Coordination for the Improvement of Higher Education Personnel (CAPES) – Brazil for the financial support.

REFERENCES

Agrell, J. Birgersson, H. Boutonnet, M. 2002 *J. Power Sources*, 2002, 106, 249-257.

Chu, Z. H. Chen; Y. Yu; Q. Wang; D. Fanga. *J. Mol. Catal. A: Chem*., 366, 2013, 48–53.

Colpini, L. M. S. G. G. Lenzi; L. Martins; E. A. U. González; O. A. A. Santos; C. M. M. Costa. *Acta Scientiarum Technol.*, 2013, 15, 139-145.

Colussi, S. L. Katta; F. Amoroso; R. J. Farrauto; A. Trovarelli. *Catal. Commun*., 47, 2014, 63–66.

E2456-06, ASTM. ASTM E2456-06 Standard Terminology for Nanotechnology, v. West Consh, 2012, 1-4.

Ereña, J. Sierra, I. M. Olazar, A. G. Gayubo; A. T. Aguayo. 2008. *Ind. Eng. Chem. Res*., 47, 2238-2247.

Fierro, G. M.L. Jacono; M. Inversi, P. Porta, F. Cioci, R. 1996. Lavecchia, *Appl Catal A:Gen*, 137, 327–348.

Figueiredo, R.T. A.L.D. Ramos; H. M. C. de Andrade; J.L.G. Fierro, *Catal. Today*, 2005, 107–108, 671–675.

Figueiredo; J. L. 1987. *R.* Ribeiro. Catálise Heterogénea, Fundação Calouste Gulbenkian, Lisboa.

Fu, W. Z. Bao; W. Ding; K. Chou; Q. Li, *Catal. Commun.*, 2011, 12, 505–509.

Fu, W. Z. Bao; W. Ding; K. Chou; Q. Li. *Catal. Commun*., 12, 6, 2011, 505–509.

Gervasini, A. Bennici, S. 2005.*Appl. Catal. A:Gen.*, 2005, 281, 199–205.

Gonçalves, G. L.M.S. Colpini; R. Menechini Neto; O.A.A. Santos; L.M.M. Jorge; M.K. Lenzi. *Int. J. Mater. Eng. Technol.*, 2013, 10, 45–65.

Guo, P. L. Chen; Q. Yang; M. Qiao; L. Hui; H. Li; H. Xu; K. Fan. *Int. J. Hydrogen Energy*, 34, 2009, 2361 - 2368.

Hakeem, A. A. J. Rajendran; F. Kapteijn; M. Makkee. *Catal. Today*, 242, 2015, 168–177.

He, L. H. Cheng; G. Liang; Y. Yu; F. Zhao, *Appl. Catal. A:Gen.*, 2013, 452, 88–93.

Henpraserttae, S. P. Limthongkul; P. Toochinda, 2010. *Monatsh. Chem.*, 141, 269–277.

Jeong, D. W. W. J. Jang; J. O. Shim; W. B. Han; H. S. Roh; U. H. Jung; W. L. Yooh. *Renew. Energ.*, 65, 2014, 102-107.

Jorge, L.M.M. 1998. Tese de Doutorado, Universidade de São Paulo.

Kanari, N. D. Mishra; I. Gaballah; B. Dupre. *Thermochim. Acta*, 410, 2004, 93-100.

Lei, H. R. Nie; J. Fei; Z. Hou, *J. Zhejiang Univ SCI-A (Applied Physics & Engineering)*, 2012, 13, 395–406.

Lenzi, G.G. C.V.B. Fávero; L.M.S. Colpini; H. Bernabe; M.L. Baesso; S. Specchia; O.A.A. Santos. 2011. *Desalination,* 270, 241-247.

Liang, S. G. Veser. *Catal. Lett*., 142, 2012, 936-945.

Nakata, Y. Yamamoto, O. K. Shimizu. *Materials Transactions*, 34, 1993, 429–437.

Nepel, T.C.M. Lopes, P.P. V.A. Paganin; E.A. Ticianelli. 2013. *Electrochim. Acta*, 88, 217–224.

Nishida, K. I. Atake; D. Li; T. Shishido; Y. Oumi; T. Sano; K. Takehira. *Appl. Catal. A:Gen*, 337, 2008, 48–57.

Oliveira, N.M.B. 2012. Dissertação de Mestrado, Universidade Estadual de Campinas.

Panyad, S. Jongpatiwut, S. Sreethawong, T. Rirksomboon, T. Osuwan, S. 2011. *Catal. Today*, 174, 59-64.

Pearson, I.M. H. Ryu; W.C. Wong, K. Nobe, 1983. *Ind. Eng. Chem. Prod. Res. Dev.*, 22, 381-382.

Pernicone, N. T. Fantinel; C. Baldan; P. Riello; F. Pina, *Appl. Catal. A:Gen.*, 2003, 240, 199-206.

Porta, P. S. De Rossi; G. Ferraris; M. Lo Jacono; G. Minelli; G. Moretti. *J. Catal*., 109, 1988, 367-377.

Sanches, S.G. 2009. Dissertação de Mestrado, Pontifícia Universidade Católica do Rio de Janeiro.

Santos, O.A.A. 1999. Tese de Doutorado, Universidade Estadual de Campinas, 1999.

Schmal, M. Catálise Heterogênea. Synergia Editora, Rio de Janeiro, 2011.

Shen, G. C. S. Fujita; S. Matsumoto; N. Takezawa. *J. Mol. Catal. A: Chem*., 124, 1997, 123-136.

Shi, L. K. Tao; R. Yang; F. Meng; C. Xing; N. Tsubaki, *Appl. Catal. A:Gen*, 2011, 401, 46– 55.

Tanaka, Y. T. Utaka; R. Kikuchi; K. Sasaki; K. Eguchi, *Appl. Catal. A:Gen.*, 2003, 238, 11-18.

Wang, B. Y. Cui; C. Wen; X. Chen; Y. Dong; W. Dai. 2016. *Appl. Catal. A: Gen.*, 509, 66–74.

Wijayapala, R. F. Yu; C. U. Pittman Jr.; T. E. Mlsna. *Appl. Catal. A: Gen*, 480, 2014, 93–99.

Zhang, L. Y. Zhang; S. Chen. *J. Fuel Chem. Technol.*, 39, 2011, 912-917.

****